Polyhedron 49 (2013) 145–150

Contents lists available at SciVerse ScienceDirect

Polyhedron

journal homepage: www.elsevier.com/locate/poly

Synthesis and crystal structure of bis [2-(4-methylphenyl)-1-phenethyl-4(1H)-quinazolinone] dichlorocopper (II)

G.Y.S.K. Swamy [a,*], K. Ravikumar [a], K.V.S. Ramakrishna [b]

[a] Laboratory of X-ray Crystallography, CSIR-Indian Institute of Chemical Technology, Hyderabad 500 007, India
[b] Center for Nuclear Magnetic Resonance, CSIR-Indian Institute of Chemical Technology, Hyderabad 500 007, India

ARTICLE INFO

Article history:
Received 23 August 2012
Accepted 3 October 2012
Available online 12 October 2012

Keywords:
Synthesis
Copper (II) complex
X-ray crystal structure
Density functional theory
NMR spectra
Antimicrobial activity

ABSTRACT

The title complex, bis [2-(4-methylphenyl)-1-phenethyl-4(1H)-quinazolinone] dichlorocopper (II) was synthesized and characterized by single-crystal and powder X-ray diffraction, IR–UV spectra, elemental analyses, ^{1}H and ^{13}C NMR and thermogravimetric analyses. Crystal structure determination reveals that the complex consists of mononuclear units with copper (II) ion coordinating in a bis-bidentate fashion. The copper (II) ion is located on the inversion center and has an octahedral coordination environment. The conformation of the dihydropyrimidine (DHPM) ring is almost planar unlike a sofa, as in the case of pure ligand. No classical hydrogen bonds were observed in the structure. The optimized geometrical parameters were calculated using the methods based on the density functional theory (DFT). A comparison of the molecular conformation and geometrical parameters obtained from the X-ray structure analysis and the theoretical study clearly indicates that the DFT calculations agree closely the X-ray structure. The investigated complex along with the ligand has been screened simultaneously for *in vitro* antibacterial and antifungal activities and compared with the drugs in use.

1. Introduction

Quinazoline, a heterocyclic compound which contains the pyrimidine nucleus is reported to have physiological and pharmacological activities and applications in the treatment of several diseases such as leprosy and mental disorders and also exhibit wide range of activities, such as anti-bacterial [1] anti-fungal [2] and anticancer [3]. Substituted quinazolines also show their potent and specific inhibitory action against leukemia cells [4]. Structure analysis of these compounds provides an opportunity to study the biological activity and its implications for the structural requirements for binding to the receptors. Further, the pirimidine ring conformation and the substituents of the ring often play a crucial role in the structure–activity relationship of the molecule [5,6]. In addition, metal-chelation to the molecule will further enhance the potential of the anti-microbial activity [7,8]. In continuation of our work on quinazolines [9], herein, we report the crystal structure, powder X-ray diffraction (PXRD), spectroscopic and thermogravimetric (TGA) analyses, geometry optimization using DFT and the antimicrobial activity of the copper (II) complex.

2. Experimental

2.1. Preparation of bis [2-(4-methylphenyl)-1-phenethyl-4(1H)-quinazolinone] dichlorocopper (II) complex (I)

The complex was prepared by dissolving 2-(4-methylphenyl)-1-phenethyl-4(1H)-quinazolinone (L) in methanol (10 mL). After stirring for 10 min added $CuCl_2{\cdot}2H_2O$ (2 mmol) (taken in 5 mL methanol), and the mixture was stirred for 20 min. Upon slow evaporation, pale green color crystals were obtained at room temperature. *Anal.* calc. for $C_{46}H_{40}N_4O_2CuCl_2$: C, 67.78; H, 4.91; N, 6.87. Found: C, 67.86; H, 4.82; N, 6.90%.

2.2. Materials and physical measurements

All materials and reagents were obtained commercially and used without purification. The elemental analyses of C, H, and N were carried out using American PE2400 II CHNS/O elemental analyzer. IR spectra were recorded on a Thermo Nicolet Nexus – 670 FT-IR spectrophotometer in the region 4000–400 cm^{-1}, using KBr pellet. Electronic spectra were obtained using Varian Cary 5000, UV–Vis spectrophotometer. Electrospray ionization-mass spectra (ESI-MS) were recorded with quadrupole time-of-flight mass spectrometer (QSTAR XL, Applied Biosystems/MDS Sciex, Foster City, CA, USA). The samples were introduced into the source by flow injection (10 μL loop) using MeOH as the mobile phase at a flow

* Corresponding author. Tel.: +91 40 27191421.
E-mail addresses: swamygundimella@yahoo.com, swamy@iict.res.in (G.Y.S.K. Swamy).

0277-5387/$ - see front matter © 2012 Elsevier Ltd. All rights reserved.
http://dx.doi.org/10.1016/j.poly.2012.10.002

rate of 30 μL/min. The thermal behavior was studied by TGA on a TGA/SDTA Mettler Toledo 851 analyzer (Zurich, Switzerland) with open alumina crucible containing sample weighing about 8–10 mg with a linear heating rate of 10 °C/min under N_2 as purge gas. Powder X-ray diffractograms were recorded on a Bruker-AXS D8-Advance, X-ray diffractometer with graphite-monochromated Cu Kα radiation (1.5406 Å) and 2θ ranging from 5° to 50° with step size 0.005° and step time 13.5 s. The diffractometer is attached with high sensitive Lynx-Eye detector. ^{1}H and ^{13}C NMR spectra were measured with Varian Unity INOVA-500 MHz and Bruker AVANCE-III 125 MHz spectrometers at ambient temperature in DMSO-d_6.

2.3. Antimicrobial activity: antibacterial and antifungal screening

The minimum inhibitory concentration (MIC) was measured by broth dilution method [10]. A Micro plate with nutrient broth media (100 μl) was added to (1–9). The test compound is dissolved in DMSO and concentration of 100 μl/ml of the test compound is added to the first well, which is serially diluted from 1–8 and the 9th well acts as a control. A fixed volume of 100 μl over night culture is added in the entire well and incubated at 37 °C for 24 h. After the incubation period the microplate was measured for turbidity with spectrophotometer (Tecan M200 infinite Microplate Reader). Penicillin and Streptomycin were used as positive control. Neutrient broth was procured from M/s Himedia Laboratories, Mumbai, India.

Agar cup bioassay (SMART (Version 5.625) [11]) was employed for testing antifungal activity. Solutions were prepared by dissolving the compound in DMSO and different concentrations (100 μg and 150 μg) were made. After inoculation, 6 mm sterile disk were scooped out with 6 mm sterile cork borer and the lids of the dishes were replaced. Controls were maintained with DMSO and Clotrimazole B (50 μg/mL). The treated and the controls were kept at 27° C for 48 h. Inhibition zones were measured and the diameter was calculated in millimeter. Three replicates were maintained for each treatment. Media Potato Dextrose broth and Potato Dextrose agar were procured from M/S Himedia Laboratories, Mumbai, India.

2.4. Crystal structure determination

X-ray single crystal data collected was performed at room temperature with a Bruker SMART Apex CCD area detector (SAINT (Version 6.28a) [12]). Preliminary lattice parameters and orientation matrices were obtained from three sets of frames. Intensity data were collected using graphite-monochromated MoKα radiation (λ = 0.71073 Å) with the ω-scan method.

Integration and scaling of intensity data were accomplished using SAINT [13] and absorption corrections were performed using SADABS [14]. The structures were solved by direct methods and refined by a full matrix least-squares procedure based on F^2 [15]. Non-hydrogen atoms were refined with anisotropic displacement parameters and hydrogen atoms were included in the models in their calculated positions in the riding model approximation. The details of the crystal data and refinement convergence are gathered in Table 1. The geometrical calculations and molecular graphics were computed using programs PARST [16], ORTEP-3 [17] and PLATON [18].

Table 1
Crystallographic data and data collection parameters.

Empirical formula	$C_{46}H_{40}N_4O_2CuCl_2$
Formula weight	815.30
Crystal system	orthorhombic
Space group	*Pbcn*
Unit cell dimensions	
a (Å)	19.0406(12)
b (Å)	9.4385(06)
c (Å)	22.5152(14)
V (Å^3)	4046.3(4)
Z	4
D_{cal} (Mg/m^3)	1.3383
μ (mm^{-1})	0.7151
Radiation (Mo Kα) (Å)	0.71073
F(000)	1692
θ range for data collection (°)	2.1–25.00
Reflections collected	27205
Independent reflections	3566
No. of reflections [$I > 2\sigma(I)$]	2994
No. of parameters	251
Final *R* indices *R*/*wR*	0.0299/0.0885
Goodness of fit on F^2	1.036
Largest difference peak and hole (e Å^{-3})	0.238, −0.153

3. Results and discussion

3.1. Analytical and spectral studies

3.1.1. IR Spectra

The IR spectra of the ligand and its Cu(II)-complex (Figs. S1 and S2, supporting information), were recorded separately. IR spectra of the complex show that the pyrimidine $\gamma_{C=N}$ stretching frequency in the free ligand at 1492 cm^{-1} shifts to 1483 cm^{-1}, which indicates that the imino nitrogen of the ligand coordinated to the Cu(II) [19]. Similarly, the $\gamma_{C=O}$ band of the quinazoline was shifted to a little higher wave number (1666–1673 cm^{-1}) indicating coordination of the carbonyl oxygen to the metal atom. This can be attributed to the minimum effect of the pyrimidine ring conjugation on the carbonyl bond (C=O 1.234(2) Å (1.231(3) Å in the ligand)). A medium intensity band appears at 3177 cm^{-1} in the ligand which is assigned to γ(NH) stretching of the quinazoline ring, completely disappeared in the complex molecule. This may be due to deprotonation of the amino nitrogen upon coordination with Cu(II). This result is further confirmed by X-ray and ^{1}H NMR studies. New bands with medium to weak intensities at 425–510 cm^{-1} are tentatively assigned to $\gamma_{(M-O)/(M-N)}$ [20].

3.1.2. Uv

The electronic spectrum of the ligand shows a strong band at 241 nm ($n \rightarrow \pi^*$) and a relatively weak band at 357 nm ($\pi \rightarrow \pi^*$) for C=O and C=N chromophores. On complexation, these bands were shifted to 206 and 306 nm respectively, indicating the metal coordination to the carbonyl oxygen and the pyrimidine nitrogen (N1) [21], agreeing with X-ray diffraction.

3.1.3. ESI – mass spectra

The positive ion ESI mass spectrum of the ligand showed the protonated molecular ion, $[M+H]^+$ at *m/z* 343 and $[M+Na]^+$ ion at *m/z* 365. The spectrum of the prepared Cu(II)-complex with the ligand did not show intact complex with two chlorides. The spectrum showed only the species without chlorides at *m/z* 743 corresponding to $[Cu+2L-2H]^+$ ion. The isotopic distribution of the ion *m/z* 743 matching well with the simulated spectrum obtained for $[C_{46}H_{40}N_4O_2Cu]^+$. The spectrum clearly confirms dehydrogenation of the ligand during complex formation as observed by X-ray diffraction. The oxidation state of Cu in the ion *m/z* 743 is +1, where the Cu might have reduced from Cu(II) to Cu(I) during ESI ionization. These assignments are based on ^{63}Cu.

3.1.4. ^{1}H and ^{13}C NMR studies. ^{1}H and ^{13}C NMR spectra of the ligand (L) (Figs. S3 and S4) and its Cu(II)-complex (Figs. S5 and S6), were recorded in DMSO-d_6 at 500 and 125 MHz respectively. The assignment of protons and carbons was made with the help of 2D NMR

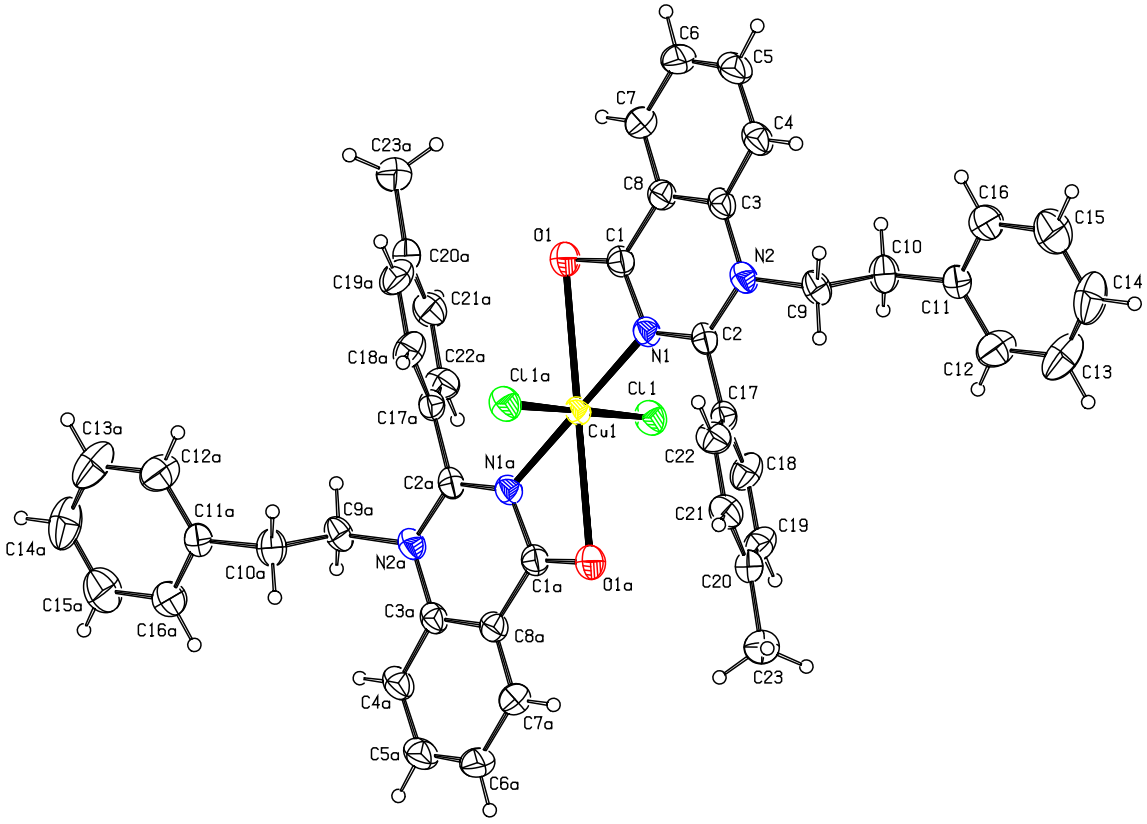

Fig. 1. Structural representation and atom-numbering scheme. Thermal ellipsoids are drawn at the 30% probability level.

Table 2
Selected geometric parameters [Å, °] by X-ray diffraction and theoretical calculations.

	Exp.	Cal.		Exp.	Cal.
C1–N1	1.407 (2)	1.402	N1–Cu1–Cl1	90.87 (4)	89.84
C1–O1	1.234 (2)	1.222	O1–Cu1– Cl1	88.70 (5)	89.87
C2–N1	1.331 (2)	1.309	C1–N1–C2	122.20 (14)	122.49
C2–N2	1.381 (2)	1.370	C1–N1–Cu1	107.38 (10)	111.58
C3–N2	1.424 (2)	1.408	C2–N1–Cu1	130.31 (11)	125.93
C9–N2	1.496 (2)	1.478	C2–N2–C3	119.98 (14)	119.57
Cu1–N1	2.025 (1)	1.992	C2–N2–C9	120.94 (14)	120.62
Cu1–Cl1	2.323 (5)	2.312	C3–N2–C9	118.32 (14)	119.76
Cu1–O1	2.740 (3)	2.865			
C17–C2–N1–C1	176.17 (15)	179.72			
C17–C2–N2–C3	175.40 (15)	179.81			
N2–C9–C10–C11	177.83 (14)	178.70			

Table 3
Hydrogen bonding geometry [Å, °].

D–H…A	D–H	H…A	D…A	D–H…A
C14–H14…O1^{i}	0.93	2.81	3.701	161.40 (**2**)
C21–H21…Cl1^{ii}	0.93	2.97	3.830	153.79 (**2**)

Symmetry code: (i) $-x+½, -y+½, z-½$; (ii) $x, y-1, z$.

(HSQC, HMBC DQFCOSY, TOCSY and NOESY). The ^{1}H and ^{13}C NMR spectral data of the ligand and the complex along with the assignments are given in Table 4. The ^{1}H NMR spectrum of the ligand (L) exhibits one doublet at 8.54 ppm, corresponding to the amine, N(1)H (D_2O exchangeable), not observed in the Cu(II)–complex ^{1}H NMR spectrum. The absence of the N(1)H resonance peak confirms the involvement of N(1)H in coordination with the metal ion via deprotonation. Similarly, a resonance peak occurs at 5.66 ppm corresponds to C(2)H in the ligand (L), disappeared in the Cu(II)–complex. This may be due to the dehydrogenation in the DHPM ring as confirmed by XRD study. The region at 6.7–7.8 ppm corresponds to hydrogens of the aromatic rings. In the spectrum of the Cu(II)–complex, the peaks were broadened in this region and shifted down field, attributed to increased conjugation on coordination [22].

3.2. Description of the crystal structure

Fig. 1 shows an Ortep drawing of the title molecule with atomic numbering scheme which was drawn at 30% probability level using Platon. Selected bond distances and angles are given in Table 2.

The complex (I) consists of mononuclear units with copper (II) ions coordinating in a bis-bidentate fashion. A perspective view is shown in Fig. 1. The copper (II) ion is located on the inversion center (Wyckoff position, 4b) and has an octahedral coordination environment. Two imine nitrogens (N1 and N1a, $a = -x$, $1-y$, $1-z$) from two different pyrimidine rings *cis* coordinate to the Cu atom in the equatorial plane with Cu–N distance of 2.025 (1) Å, while two carbonyl oxygens (O1 and O1a) occupy the other *cis* sites in the equatorial plane with Cu–O bonds of 2.740 (3) Å. The axial sites are occupied by two chlorine atoms (Cl1 and Cl1a) with Cu–Cl distances of 2.323 (1) Å to complete six coordination. The long distances of Cu–O bonds compare to other four coordination bonds indicate the existence of the Jahn–Teller elongation effect. The bite angle of the chelating ligand is 78.9 (4)°.

The DHPM ring in the pure ligand adopts a sofa conformation [9] due to the effect of conjugation, where as in the present complex, the ring is almost planar (an average deviation of 0.0089 Å from the least squares plane) though it has some effect of conjugation (the formal single bonds N1–C2 and N2–C2 have partial

Table 4
^{1}H and ^{13}C NMR chemical shift data of the ligand (L) and its Cu(II)–complex (in ppm).

Ligand (L)	Cu(II)–complex
8.54, (d, *J* = 3.8 Hz, 1H, N(1)H)	–
7.68 (127.8), (dd, *J* = 1.6, 7.6 Hz, 1H, C(7)H)	8.17 (127.4), (d, *J* = 7.5 Hz, 1H, C(7)H)
7.38 (133.9) (m, 1H, C(5)H)	7.97 (117.0), (d, *J* = 8.5 Hz, 1H, C(4)H)
7.27 (128.2), (m, 2H, C(15)H–C(17)H)	7.92 (133.7), (t, *J* = 7.5 Hz, 1H, C(6)H)
7.22 (128.6), (m, 3H, C(12)H,C(14)H, C(16)H)	7.61 (125.9), (t, *J* = 7.0 Hz, 1H, C(5)H)
7.18 (126.3), (d, *J* = 8.5 Hz, 2H, C(18)H, C(19)H)	7.29 (128.4), (m, 2H, C(18)H–C(19)H)
7.11 (128.8), (d, *J* = 7.6 Hz, 2H, C(21)H–C(22)H)	7.24 (127.5), (m, 2H, C(21)H–C(22)H)
6.90 (112.6), (d, *J* = 8.4 Hz, 1H, C(4)H)	7.17 (128.2), (m, 3H, C(13)H, C(13)H, C(15)H)
6.72 (116.9), (d, *J* = 8.4 Hz, 1H, C(6)H)	6.76 (128.4), (d, *J* = 7.5 Hz, 2H, C(12)H, C(16)H)
5.66 (70.6), (d, *J* = 3.8 Hz, 1H, C(2)H)	–
3.67 (50.0), (m, 1H, C(9)H)	4.40 (50.0), (m, 2H, C(9)H, C(9′)H)
3.28 (50.0), (m, 1H, C(9′)H)	
2.86 (32.7), (m, 1H, C(10)H)	2.90 (33.2), (m, 2H, C(10)H, C(10′)H)
2.72 (32.7), (m, 1H, C(10′)H)	
2.23 (20.7), (s, 3H, C(23)H_3)	2.40 (20.7), (s, 3H, C(23)H_3)

double bond character and are shorter than the typical Csp^2–N bond distance (1.426 Å)) [23]. One of the reasons for the planarity of the DHPM ring may be due to the ligand–metal complexation through the atoms N1 and O1 of the DHPM ring. In other words, the strain in the ligand (DHPM ring) is very much restricted to minimum due to ligand–metal complexation. Further, on complexation of the ligand to the metal atom, some dehydrogenation has been observed (Sp^3 becomes Sp^2 (atom C2)) in the DHPM ring. Aromaticity may be the driving force for it.

Table 5
Antibacterial activity of the quinazolinone ligand and its Cu(II)–complex.

Compound	BS (MIC μg/mL)	SA (MIC μg/mL)	SE (MIC μg/mL)	EC (MIC μg/mL)	PA (MIC μg/mL)	KE (MIC μg/mL)
Ligand	150	150	150	150	150	150
Cu-complex	150	75	150	150	18.75	150
Penicillin	1.562	1.562	3.125	12.5	12.5	6.25
Streptomycin	6.25	6.25	3.125	6.25	1.562	3.125

BS = *B. subtilis*; SA = *S. aureus*; SE = *S. epidermidis*; EC = *E. coli*; PA = *P. aeruginosa*; KP = *K. pneumoniae*.

It has been reported that, more the planarity of the DHPM ring higher the pharmacological activity of the molecule [5]. In the present structure, we have observed that the structure–activity correlation was supported by two important points. The first one, DHPM ring planarity and the second one is ligand–metal complexation. It is important to note that, on complexation with the metal, the planarity of the DHPM ring increased drastically (average deviation of the atoms N1, N2, C1–C3, C8 from the l.s. plane is 0.0089 Å as compared to the ligand, 0.105 Å) which in turn increased moderately, the antibacterial activity (Table 5). As stated by several researchers [24–27] the metal chelates exhibit more inhibitory effects than the parent ligands due to the increasing lipophilic character of the metal chelate which in turn responsible for their enhanced potent antibacterial activity.

The phenethyl group in the molecule has a fully extended conformation with respect to the central pyrimidine ring (Table 2). The sum of the bond angles around the atoms N1 (359.9°) and N2 (359.2°) indicate the pyramidal configuration. It is interesting to note that, the *p*-tolyl group is positioned equatorially at C2 (average torsion angle of C1–N1–C2–C17 & C3–N2–C2–C17 is 175.79(15)°), while in the ligand it is oriented axially (89.4(2)°).

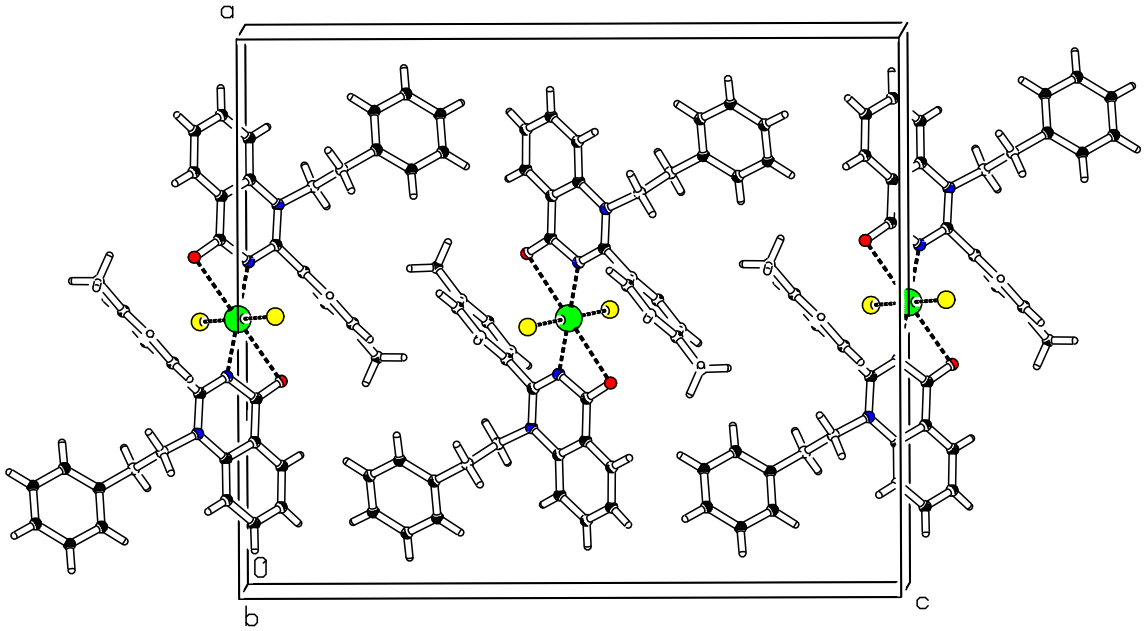

Fig. 2. Crystal packing in the unit cell viewed down the [010] axis.

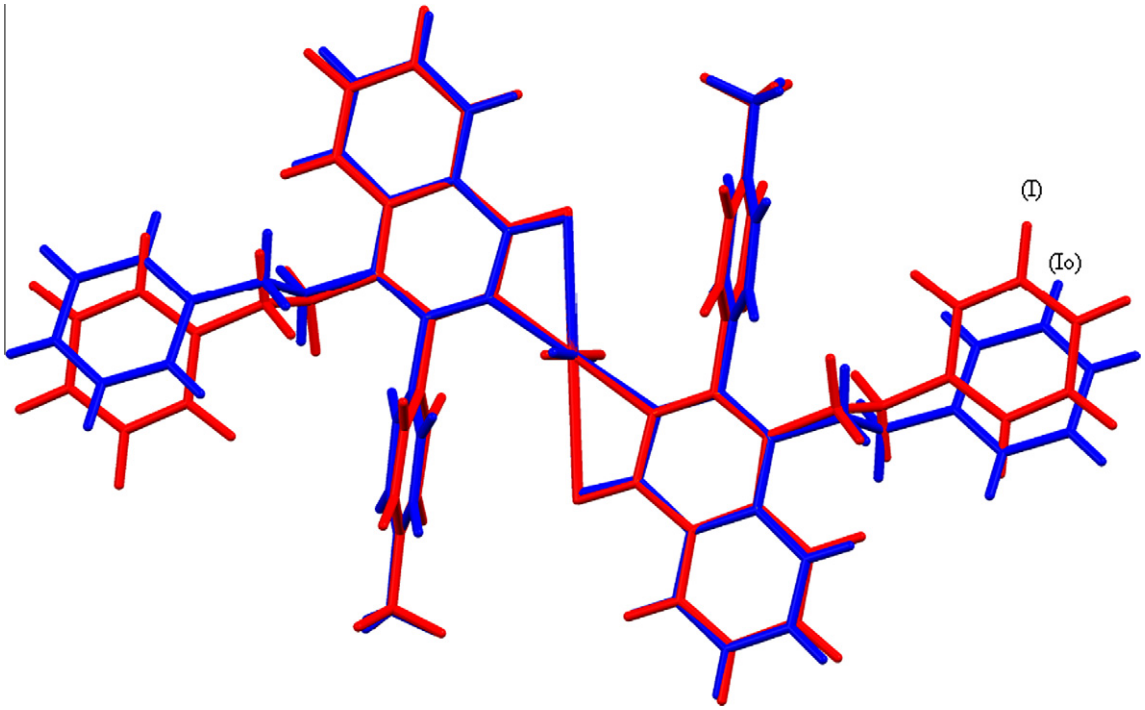

Fig. 3. A superposition of the molecular conformations of the title molecule (I) and its optimized structure (II). The overlay was made by making a least-squares fit through DHPM ring of (I). The r.m.s. deviation with respect to the conformation of (I) (red in the electronic version of the journal) is 0.091 (Io – blue) (color online).

No classical hydrogen bonds were found in the structure (Fig. 2). The crystal lattice is stabilized by C–H...O and van der Waals interactions. The structure contains a number of intermolecular C–H...X contacts with H...X being well within the van der Waals radii (those with C–H...X angle above 100° are listed in Table 3). The intermolecular contacts may be regarded as weak non-classical C–H...O hydrogen bonds, but their contribution to the overall lattice energy must be very small.

3.3. Optimised geometry

DFT calculations were performed using the crystallographic structure parameters of the Cu(II)–complex as a starting point. The DFT method was applied at the B3LYP hybrid exchange correlation function level [28,29] using the 6–31G(d,p) basis set [30] as implemented in GAUSSIAN03 [31]. The combination of hybrid exchange functional and correlation functional known as B3LYP has been widely used for several metal complexes [32–34]. The optimized geometric parameters for some selected bond lengths and angles are given in Table 2 and represent the molecule in the gas-phase like orientation. The DFT calculations predict the average C–N bond length to be 1.393 Å, which is slightly less than the experimentally obtained value 1.406 Å. The calculated Cu1–O1 bond length is 2.865 Å, while the experimental value is slightly less (2.740 Å). Similarly, there is a variation of 0.32–4.4° in the bond angles around the atoms N1 and N2 between the calculated and experimental values (Table 2). In addition, the orientation of the p-tolyl group with respect to DHPM ring (experimental av. torsion angles of C17–C2–N1–C1 and C17–C2–N2–C3 175.79 (15)°) is also slightly effected (cal. value 179.77°). These discrepancies between the calculated and the crystallographically determined values may be accounted for by solid-state packing effects in the crystal structure of the title molecule, which are not included in the gas-phase DFT structure optimization. A superposition of the molecular conformation of both the geometries (experimental and theoretical) is shown in the Fig. 3. The overlay was made by making a least-squares fit through the DHPM ring of the title molecule (see scheme 1).

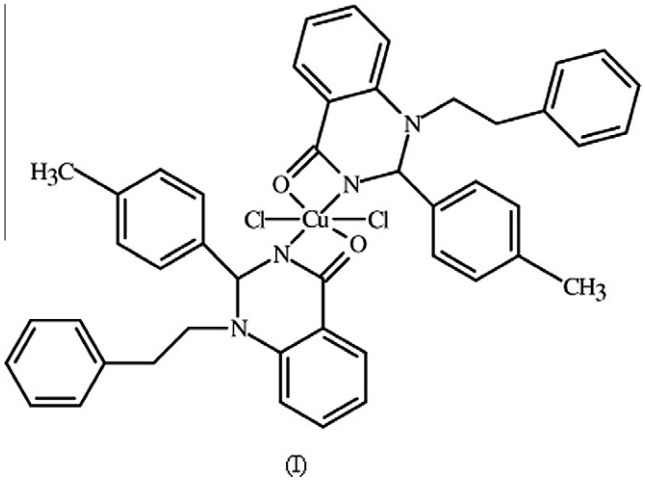

(I)

Scheme 1.

3.4. PXRD measurement

The simulated and experimental PXRD patterns of Cu(II)–complex (Fig. S7) are in agreement with each other. It was found a few additional peaks and some differences in the intensities between the peaks of the patterns. This may be attributed to a very minor quantity of an impurity phase and the effect of preferred orientation of the powder sample.

3.5. Thermal studies

The thermogravimetric (TG) curve (Fig. S8), of the title compound exhibits a two step of weight loss from 30 to 800 °C.

The initial weight loss of 8.72% (calc.: 8.69%) in the temperature range 100–250 °C is due to the loss of two chlorides in the molecule. The next weight loss of 84.4% (calc.: 84.1%), in the range 250–550 °C is due to loss of two ligands. A plateau is obtained after heating the complex above 550 °C up to 800 °C, which corresponds to the final residuals and the formation of stable CuO.

3.6. Antimicrobial screening

Both the ligand and the copper(II)–complex were subjected to antimicrobial screening. The results show that the complex exhibit more inhibitory effects than the parent ligand. The activity of the ligand and the metal complex was tested against some pathogenic test organism including Gram-positive (*B. subtilis*, *S. aureus* and *S. epidermidis*), Gram-negative (*E.coli*, *P. aeruginosa* and *K. pneumoniae*) by the micro dilution (DMSO as solvent) method. One can see from the results of the antibacterial screening (Table 5), that the ligand has hardly any activity against the tested bacteria. Where as the copper complex inhibits the growth of *S. aureus* and *P. aeruginosa* even at low concentration (18 μg/mL). Further, the ligand and the complex were tested for their antifungal activity against some test organism (*A. niger*, *S. cerevisiae*, *C. rugosa* and *C. albicans*). The results show neither the ligand nor the complex has any activity.

4. Conclusion

We have reported the synthesis and characterization of quinazolinone–Cu(II) complex. The results of the single crystal X-ray structure analysis were supported by elemental, thermal, ESI-mass, IR, PXRD, DFT, ^{1}H and ^{13}C NMR and electronic spectral studies. In the light of structure–activity relationship of the title molecule, we have observed two important points which are inter-related and may be responsible for the pro-activity of the title molecule. That is, (i) DHPM ring planarity, and (ii) metal complexation. Further, antimicrobial studies of the Cu(II)–complex also show some encouraging results against the some tested bacterial strains.

Acknowledgements

The authors are thankful to Dr. U. S. N. Murthy, Head, Biology Dept. IICT for antimicrobial data, Dr. N. Jagadeesh Babu, X-ray Crystallography center, IICT for the theoretical calculations and Dr. J. S. Yadav, Director, IICT, Hyderabad for his kind encouragement.

Appendix A. Supplementary data

CCDC **812390** contains the supplementary crystallographic data for the title molecule. These data can be obtained free of charge via http://www.ccdc.cam.ac.uk/conts/retrieving.html, or from the Cambridge Crystallographic Data Centre, 12 Union Road, Cambridge CB2 1EZ, UK; fax: +44 1223 336 033; or e-mail: deposit@ccdc.cam.ac.uk. Supplementary data associated with this article can be found, in the online version, at http://dx.doi.org/10.1016/j.poly.2012.10.002.

References

[1] G.K. Nesrin, K. Semra, Y. Samiye, Y. Kemal, O. Ozen, U. Gulberk, E. Kevser, K. Engin, Y. Akgul, Bioorg. Med. Chem. 17 (2009) 675.
[2] A. Dandia, R. Singh, P. Sarawagi, J. Fluorine Chem. 125 (2004) 1835.
[3] M.J. Hour, L.J. Huang, S.C. Kuo, Y. Xia, K. Bastow, Y. Nakanishi, E. Hamel, K.H. Lee, J. Med. Chem. 43 (2000) 4479.
[4] K. Tamura, M. Fukuoka, Int. J. Clin. Oncol. 8 (2003) 207.
[5] R. Fossheim, K. Svarteng, A. Mostad, C. Romming, E. Shefter, D.J. Triggle, J. Med. Chem. 25 (1982) 126.
[6] G.Y.S.K. Swamy, B. Sridhar, K. Ravikumar, Y.S. Sadanandam, Acta Crystallogr. Sect. C64 (2008) o80.
[7] K.B. Gudasi, S.A. Patil, M.V. Kulkarni, M. Nethaji, Transition Met. Chem. 34 (2009) 325.
[8] A.A.H. Al-Amiery, Y.K. Al-Majedy, S.A. Abdulhadi, A.H. Sadoon, Afr. J. Pure Appl. Chem. 3 (2009) 218.
[9] G.Y.S.K. Swamy, K. Ravikumar, J. Chem. Crystallogr. 35 (2005) 183.
[10] National Committee for Clinical Laboratory Standards, Methods for Dilution Antimicrobial Susceptibility Tests for Bacteria, which Grows Aerobically, fifth ed., Approved Standard M7-A5, NCCLs, Villanova, PA, 2000.
[11] M.E. Linday, Practical Introduction to Microbiology, E. and F. N. Spon Ltd., UK, 1962.
[12] Bruker SMART (Version 5.625), Bruker AXS Inc., Madison, WI, USA, 2001.
[13] Bruker SAINT (Version 6.28a), Bruker AXS Inc., Madison, WI, USA, 2001.
[14] G.M. Sheldrick, SADABS. Program for Empirical Absorption Correction of Area Detector Data, Univ. of Gottingen, Germany, 1996.
[15] G.M. Sheldrick, Acta Crystallogr. Sect. A64 (2008) 112.
[16] M.J. Nardelli, J. Appl. Crystallogr. 28 (1995) 659.
[17] L.J. Farrugia, J. Appl. Crystallogr. 30 (1997) 565.
[18] A.L. Spek, J. Appl. Crystallogr. 36 (2003) 7.
[19] K.B. Gudasi, S.A. Patil, R.S. Vadavi, R.V. Shenoy, M. Nethaji, Transition Met. Chem. 31 (2006) 586.
[20] K. Nakamoto, Infrared and Raman Spectra of Inorganic and Coordination Compounds, fifth ed., Wiley, New York, 1997.
[21] M. Sonmez, A. Levent, M. Sekerci, Russ. J. Coord. Chem. 30 (2004) 655.
[22] A.M. Khedr, D.F. Draz, J. Coord. Chem. 63 (2010) 1418.
[23] A. Lorente, C. Galan, I. Fonswca, J. Sanz-Aparico, Can. J. Chem. 73 (1995) 1546.
[24] R.S. Hoonur, B.R. Patil, D.S. Badiger, R.S. Vadavi, K.B. Gudasi, P.R. Dandawate, M.M. Ghaisas, S.B. Padhye, M. Nethaji, Eur. J. Med. Chem. 45 (2010) 2277.
[25] M.B. Halli, V.B. Patil, K. Mallikarjun, R.B. Sumathi, J. Coord. Chem. 64 (2011) 651.
[26] M. Konstandinidou, A. Kourounakis, M. Yiangou, L. Hadjipetrou, D. Kovalademertzi, S. Hadjikakou, M. Demertzis, J. Inorg. Biochem. 70 (1998) 63.
[27] K.B. Gudasi, R.S. Vadavi, R.V. Shenoy, M.S. Patil, S.A. Patil, M. Nethaji, Transition Met. Chem. 31 (2006) 374.
[28] A.D. Becke, Chem. Phys. 98 (1993) 5648.
[29] C. Lee, W. Yang, R.G. Parr, Phys. Rev. B37 (1988) 785.
[30] C.W. Bauschlicher, H. Partridge, Chem. Phys. Lett. 240 (1995) 533.
[31] M.J. Frisch et al., Gaussian 03, Revision C01, Wallingford, CT, USA, 2004.
[32] I.V. Khavrutskii, D.G. Musaey, K. Morokuma, Inorg. Chem. 42 (2003) 2606.
[33] T. Kar, M.-S. Liao, S. Biswas, S. Sarkar, K. Dey, G.P.A. Yap, K. Kreisel, Spectrochim. Acta Part A 65 (2006) 882.
[34] Y.-P. Tong, Y.-W. Lin, Inorg. Chim. Acta 362 (2009) 2167.